ACS OMEGA

Article

Cite This: ACS Omega 2018, 3, 86−95

Biocompatible Chitosan-Functionalized Upconverting Nanocomposites

Hau Van Duong,[†,‡] Trang The Lieu Chau,[†] Nhan Thi Thanh Dang,[§] Frankie Vanterpool,[∥] Manuel Salmerón-Sánchez,[∥] Erlantz Lizundia,[⊥] Hoa Thai Tran,*[,†] Long Viet Nguyen,*[,#,▽,◆] and Thanh-Dinh Nguyen*[,○]

[†]Department of Chemistry, Hue University of Sciences, Hue University, 77 Nguyen Hue, Hue 530000, Vietnam

[‡]Department of Chemistry, Hue University of Agriculture and Forestry, Hue University, 102 Phung Hung, Hue 530000, Vietnam

[§]Department of Chemistry, Hue University of Education, Hue University, 34 Le Loi, Hue 530000, Vietnam

[∥]Division of Biomedical Engineering, School of Engineering, University of Glasgow, Glasgow G12 8QQ, U.K.

[⊥]Department of Graphic Design and Engineering Projects, Bilbao Faculty of Engineering, University of the Basque Country (UPV/EHU), Bilbao 48013, Spain

[#]Ceramics and Biomaterials Research Group and [▽]Faculty of Applied Sciences, Ton Duc Thang University, Ho Chi Minh City 71000, Vietnam

[○]Department of Chemistry, University of British Columbia, 2036 Main Mall, Vancouver, British Columbia V6T 1Z1, Canada

Supporting Information

ABSTRACT: Simultaneous integration of photon emission and biocompatibility into nanoparticles is an interesting strategy to develop applications of advanced optical materials. In this work, we present the synthesis of biocompatible optical nanocomposites from the combination of near-infrared luminescent lanthanide nanoparticles and water-soluble chitosan. $NaYF_4$:Yb,Er upconverting nanocrystal guests and water-soluble chitosan hosts are prepared and integrated together into biofunctional optical composites. The control of aqueous dissolution, gelation, assembly, and drying of $NaYF_4$:Yb,Er nanocolloids and chitosan liquids allowed us to design novel optical structures of spongelike aerogels and beadlike microspheres. Well-defined shape and near-infrared response lead upconverting nanocrystals to serve as photon converters to couple with plasmonic gold (Au) nanoparticles. Biocompatible chitosan-stabilized Au/$NaYF_4$:Yb,Er nanocomposites are prepared to show their potential use in biomedicine as we find them exhibiting a half-maximal effective concentration (EC_{50}) of 0.58 mg mL^{-1} for chitosan-stabilized Au/$NaYF_4$:Yb,Er nanorods versus 0.24 mg mL^{-1} for chitosan-stabilized $NaYF_4$:Yb,Er after 24 h. As a result of their low cytotoxicity and upconverting response, these novel materials hold promise to be interesting for biomedicine, analytical sensing, and other applications.

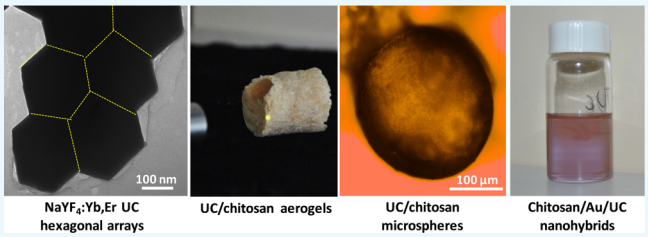

1. INTRODUCTION

Biocompatible optical nanomaterials are of interest as smart tools for applications in many fields of science and healthcare technologies.[1,2] There has been an increasing demand for fabricating functional devices from these materials. In this framework, light-sensitive nanocomponents and biopolymers are considered as novel substances to combine together into promising nanocomposites.[3] The optical and biocompatible responses endow these composites with a wide range of desirable properties for their prospective use in medicine, bioimaging, sensing, adsorption, and photocatalysis.[4] A great potential of these composites is useful for biomedical imaging because of low cytotoxicity of biopolymers and sensitive response of optical nanoelements.[5] It is of key importance to manipulate the surface, morphological, and structural features of the integrated materials to obtain a homogeneous incorporation of the functional components for improving their reaction performance.[6] With multiple-purpose applications, attempts of fabricating biocompatible optical nanocomposites with different structural forms, such as spongelike aerogels, beadlike spheres, hybrids, or water-dispersible colloids, are of great significance to the scientific community.

Upconverting (UC) materials can absorb photons and emit visible light after excitation by near-infrared (NIR) light.[7] The NIR-emitting luminescence is known to be a photophysical process of photon UC emission. $NaYF_4$:Yb,Er is a well-known UC material composed of an insulating $NaYF_4$ host and Yb^{3+} and Er^{3+} dopants incorporated into the matrix lattice.[8] Remarkably, $NaYF_4$:Yb,Er UC nanocrystals can convert near-infrared light to visible light through lanthanide (Yb^{3+} and Er^{3+})

Received: September 13, 2017
Accepted: December 18, 2017
Published: January 4, 2018

DOI: 10.1021/acsomega.7b01355
ACS Omega 2018, 3, 86−95

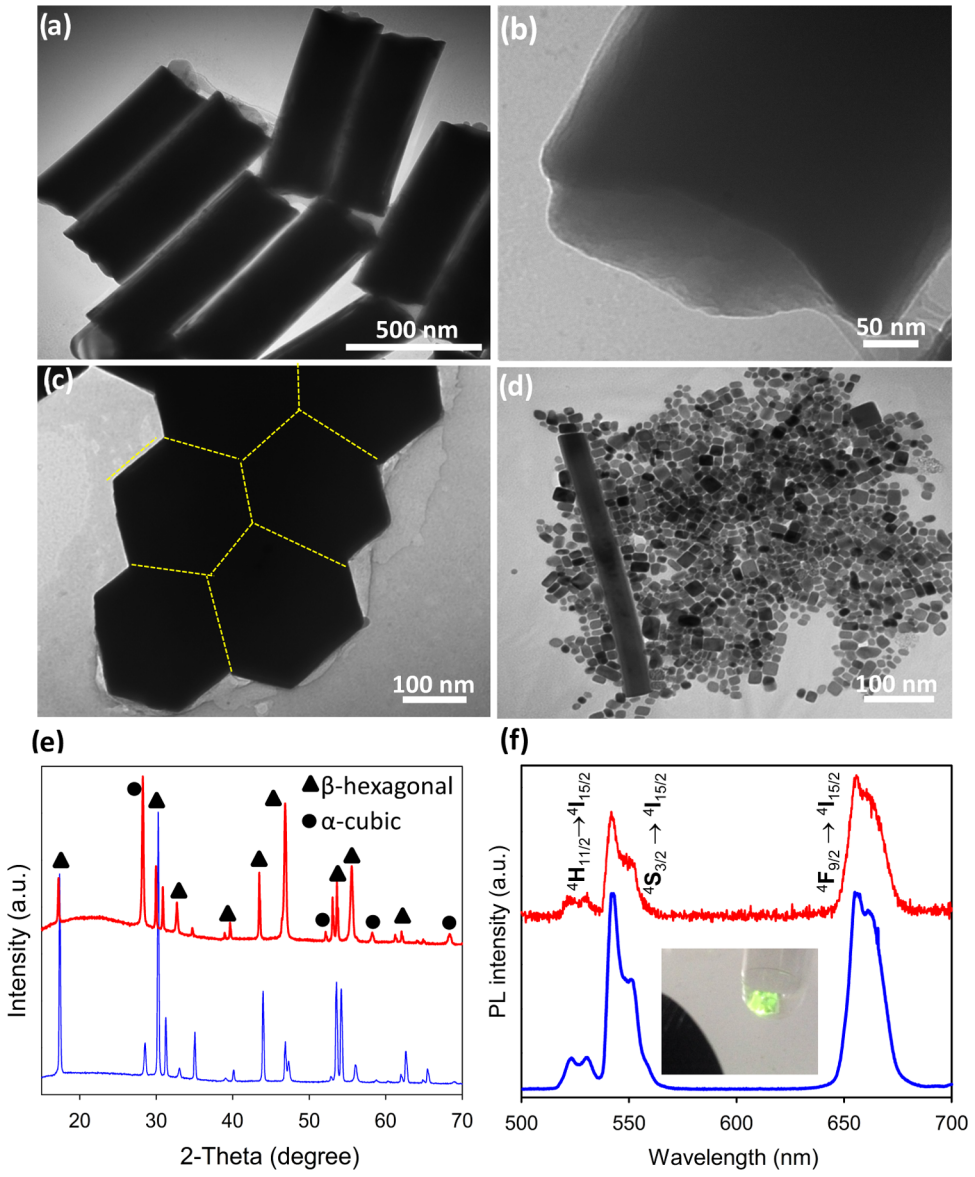

Figure 1. Shape-controlled synthesis of OA-capped $NaYF_4$:Yb,Er UC nanocrystals. (a) Transmission electron microscopy (TEM) image of UC hexagonal nanorod arrays, (b) TEM image of an individual UC hexagonal nanorod viewed along its tip, (c) TEM image viewed along a tip of assembled UC hexagonal nanorods showing concave surfaces, (d) TEM image of cube-/rod-shaped UC nanocrystals, (e) PXRD patterns, and (f) UC photoluminescence (PL) spectra of $NaYF_4$:Yb,Er hexagonal nanorods (red) and $NaYF_4$:Yb,Er cube-/rod-shaped nanocrystals (blue). The inset shows a photo of UC hexagonal nanorod powders emitting brilliant green color under 980 nm laser excitation.

doping, attributed to energy transfer pathways by dopant−host interactions.[7] Thanks to structure-dependent photon efficiency, the control of the size, shape, and crystallinity of the $NaYF_4$:Yb,Er UC nanomaterials would enable the development of optical bioprobes with improved performance.[9,10] Accordingly, the low-energy light absorption, high sensitivity, low toxicity, and structural stability make $NaYF_4$:Yb,Er UC nanoparticles useful as novel photon upconverters to fabricating advanced optical materials for applications in biomedical imaging, security labeling, and energy conversion.[11−14]

Chitosan is the deacetylated derivative of chitin as a major biopolymer component present in the shells of crustaceans[15] and in the cell walls of some fungal species.[16] The alkaline deacetylation of natural chitin generates polycationic networks of chitosan nanofibrils with exposed primary amine groups, which are capable of enhancing the chemical reactivity for surface functionalization. As an abundant biopolymer on the earth, many attempted syntheses have used chitosan-based materials as an aqueous stabilizer for nanoparticles,[17] a fibril precursor for bioplastics and gels,[18−20] and a polymer template for hierarchical porous materials.[21] The aqueous solubility, low cytotoxicity, and polycation of chitosan are crucial factors in determining the efficiency of their derivatives in biomedicine. Regarding the potential for drug delivery and cellular imaging, cationic chitosan-based components have been proven to present stronger electrostatic interactions with anionic cell membranes, which facilitates cellular uptake.[22] This behavior, combined with its low cytotoxic response, often results in materials with potential biomedical applications. Another interesting aspect is the homogeneous solubility of native chitosan nanofibrils in water as they typically dissolve in acidic media by surface protonation. It is thus desirable to obtain neutral aqueous liquids of native chitosan and use them as either a particle stabilizer or gelling agent for biocompatible

DOI: 10.1021/acsomega.7b01355
ACS Omega 2018, 3, 86−95

optical nanocomposites to enhance their applications in the field of biomedicine.[23−25] One notable example of this subject has been reported by Duan et al.[26] on the use of the freezing−thawing process of chitosan/alkali/urea solutions to prepare biocompatible chitosan hydrogels for controlled drug release applications.

To achieve the potential of optical materials for bioimaging and analytical sensing, it is of interest to combine luminescent $NaYF_4$:Yb,Er UC nanoparticles with water-soluble chitosan into chitosan-coated UC nanocomposites. It is also interesting to control the host−guest interactions of these functional components by dispersibility, self-assembly, and solidification to design biocompatible optical nanocomposites with different structures and compositions for extending their potential uses.[27] To date, several efforts have been made to prepare chitosan-functionalized $NaYF_4$:Yb,Er nanoparticles for near-infrared photodynamic therapy.[28,29] However, there are limited descriptions on the preparation of aerogels and microspheres of $NaYF_4$:Yb,Er nanoparticles supported by water-soluble chitosan.

Herein, we report the synthesis of well-defined $NaYF_4$:Yb,Er UC nanocrystals and the subsequent coating with water-soluble chitosan to generate biocompatible optical nanocomposites. This combination is based on aqueous stabilization, gelation, solidification, and assembled confinement to fabricate $NaYF_4$:Yb,Er/chitosan aerogels, microspheres, and hybrid materials. The cytotoxic responses of chitosan-stabilized Au/$NaYF_4$:Yb,Er nanocomposites in comparison to those of chitosan-stabilized $NaYF_4$:Yb,Er nanoparticles were tested to show their potential use in biomedical applications.

2. RESULTS AND DISCUSSION

Hydrothermal treatment of a basic solution of lanthanide nitrates, sodium fluoride, and oleic acid (OA) in a water/ethanol mixture at 190 °C yielded OA-capped $NaYF_4$ UC nanocrystals codoped with 20 wt % Yb^{3+} and 2 wt % Er^{3+} (Figure S1a). We found that the precursor concentration and reaction time have a major influence on the morphological distribution of the as-prepared UC nanocrystals. Scanning electron microscopy (SEM) images in Figure 1a−c show that the UC nanocrystals are uniform single-crystalline hexagonal nanorods with concave ends having 150 nm sized six facets and ∼800 nm length. The synthetic product is a particle mixture of 20 nm sized cubes and ∼100 × 1500 nm^2 sized rods when the precursor concentration used is 2 times greater than that of the UC hexagonal nanorods (Figure 1d). This shape variation is related to the evolution gradient of monomers in the bulk solution.[30] Energy-dispersive X-ray (EDX) analyses (Figure S1b) confirm the presence of Na, F, Y, Yb, and Er with a similar atomic ratio in these UC nanoparticles prepared using the low and high precursor concentrations. Powder X-ray diffraction (PXRD) analyses (Figure 1e) show a binary mixture of a major hexagonal β-phase and a minor cubic α-phase in highly crystalline $NaYF_4$:Yb,Er hexagonal nanorods.[31] Conversely, the cube-/rod-shaped $NaYF_4$:Yb,Er nanoparticles contain the cubic α-phase predominantly rather than the hexagonal β-phase. The relative intensity of the (100) diffraction peak of the $NaYF_4$:Yb,Er hexagonal nanorods is much larger than that of the $NaYF_4$:Yb,Er cubes/nanorods, suggesting that the elongation axis of the hexagonal nanorods is along the [100] direction. Note that in the $NaYF_4$:Yb,Er structure the β-hexagonal phase is thermodynamically stable, whereas the α-cube phase is metastable. There is thus a crystal transition of an α-cube phase to a β-hexagonal phase in the $NaYF_4$:Yb,Er UC nanoparticles prepared upon extended heating.

The OA-capped $NaYF_4$:Yb,Er UC nanocrystals emit brilliant green light when excited under near-infrared laser light (980 nm), where the hexagonal nanorods exhibit stronger emission than the cubes/nanorods (inset of Figure 1f). Photoluminescence spectra (Figure 1f) of the OA-capped $NaYF_4$:Yb,Er hexagonal nanorods under 980 nm laser excitation show three main emission peaks at 522.5, 541.5, and 655.5 nm as a result of the $^4H_{11/2}-{}^4I_{15/2}$ (green), $^4S_{3/2}-{}^4I_{15/2}$ (green), and $^4F_{9/2}-{}^4I_{15/2}$ (red) UC transitions, respectively, of Er^{3+} dopants.[32] The OA-capped UC nanocube/rods also exhibit three main peaks at the same wavelengths as in the OA-capped UC hexagonal nanorods but display a lower emission intensity. The appearance of the enhanced photoluminescence in the $NaYF_4$:Yb,Er hexagonal nanorods is due to the β-hexagonal phase being predominant than the α-cubic one.

The well-defined $NaYF_4$:Yb,Er hexagonal nanorods with sensitive NIR photoresponse can be used as novel converters for the design of functional optical materials. Much progress has been made toward achieving structural diversity of the $NaYF_4$:Yb,Er-based nanomaterials for a variety of applications.[33] Notable examples are metal−organic framework/$NaYF_4$:Ln core−shells for NIR-enhanced photocatalysis,[34] $NaYF_4$:Yb,Er nanoparticles for latent fingerprints,[35] $NaYF_4$:Yb,Er UC/magnetite/dye nanocomposites for oxygen sensing,[36] lipid-coated $NaYF_4$:Yb,Er nanoparticles for bioimaging and gene delivery,[37] and CdSe/$NaYF_4$:Yb,Er nanohybrids for photovoltaics.[38] Owing to the inherent characteristics of low-energy light absorption with minimal cell damage, the $NaYF_4$:Yb,Er nanoparticles are extensively used in biomedicine. The goal of this strategy is limited to the cytotoxicity of the lanthanide-doped UC nanoparticles with biopolymers to achieve the biocompatibility. Consequently, we combined the $NaYF_4$:Yb,Er-based hexagonal nanorods with water-soluble chitosan to design different structural types of biocompatible optical composites.

We found that water-soluble chitosan macromolecules could be prepared by acetylation of native chitosan nanofibrils with acetic anhydride and sequential dissolution of acetylated chitosan in water to form an optically clear aqueous solution. This solubility is different from that of conventional chitosan prepared by alkaline deacetylation of chitin as it often does not dissolve in water because of the high crystallinity of the fibrils.[39] It is noteworthy that our acetylation procedure can yield the homogeneous aqueous solution of chitosan polymorphs rather than crystalline fibrils as confirmed by PXRD (Figure S2). The acetylation-induced aqueous dissolution of chitosan is assumed to present disrupted hydrogen bonding within the fibrils, leading to the decreased crystallinity. As a result, the acetylated chitosan fibrils swell dramatically in water and then fully dissolve to form a viscous polymeric liquid.

The hydrophobic surface of the OA-capped $NaYF_4$:Yb,Er nanoparticles renders them dispersible in nonpolar solvents, but they could not be in the form of the aqueous dispersion. The surface modification of the as-prepared $NaYF_4$:Yb,Er nanoparticles with hydrophilic and biocompatible properties is thus an important step to extend their potential to biomedicine. We prepared the aqueous dispersion of chitosan-stabilized $NaYF_4$:Yb,Er nanoparticles by sequential coating of the OA-capped UC colloids with ethylene glycol and water-soluble chitosan. Remarkably, the resulting $NaYF_4$:Yb,Er nanoparticles became dispersible in water as the aqueous colloidal solution

DOI: 10.1021/acsomega.7b01355
ACS Omega 2018, 3, 86−95

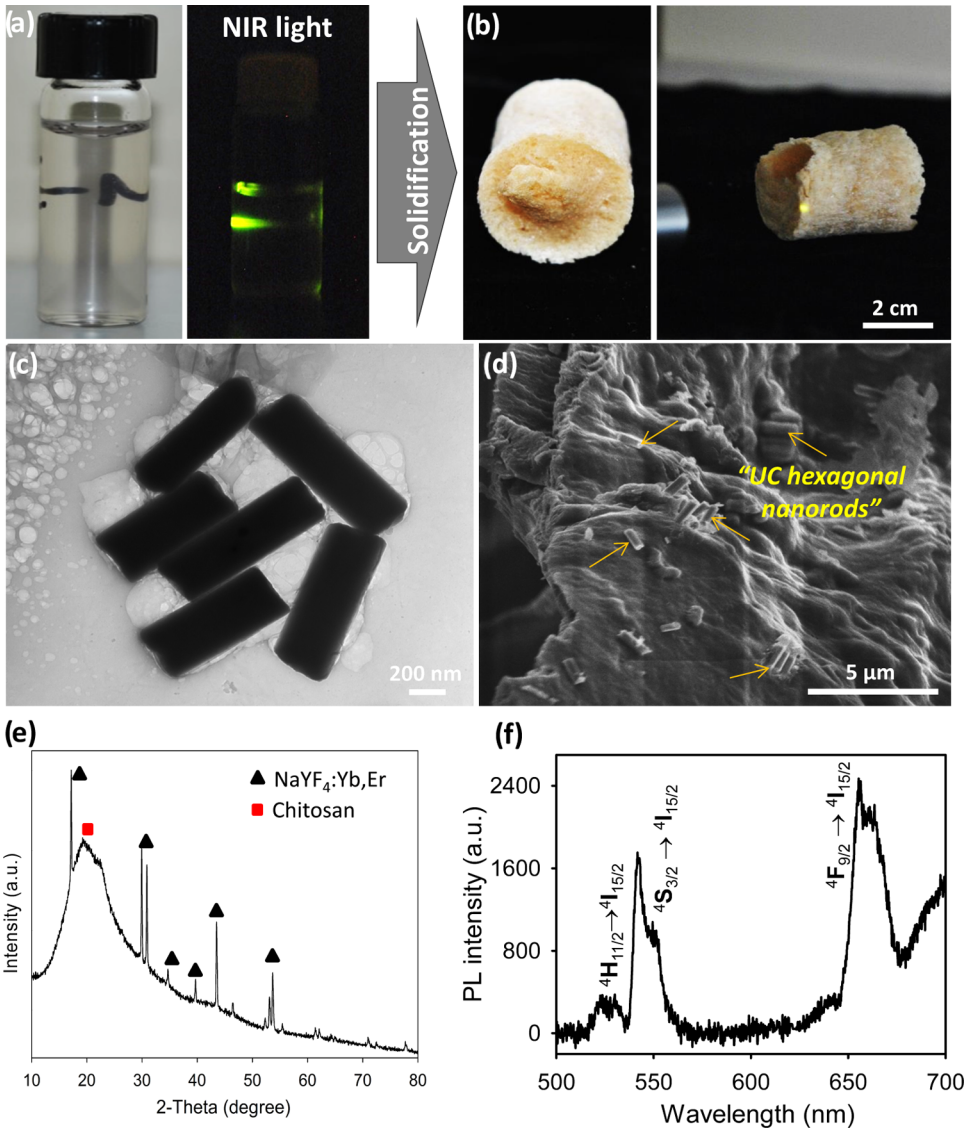

Figure 2. Formation of aerogel composites from water-soluble chitosan and $NaYF_4$:Yb,Er UC hexagonal nanorods. (a) Photos of UC/chitosan aqueous dispersion under visible light (left) and under NIR light (right), (b) photos of UC/chitosan aerogel composites under visible light (left) and NIR light (right), (c) TEM image of the UC/chitosan aqueous dispersion, (d) SEM image of UC/chitosan aerogel composites, (e) PXRD pattern, and (f) UC photoluminescence spectrum of UC/chitosan aerogel composites.

can be stable for several months (Figure S11). Infrared spectra (Figure S3) of the functionalized UC nanoparticles show distinct stretching bands of amides and hydroxyls, verifying that the OA-capped nanoparticles adsorbed with chitosan. Notably, the surface coating of the OA-capped $NaYF_4$:Yb,Er nanocolloids with water-soluble chitosan mostly retains the morphological, dispersible, and optical features (Figures 2c and S4).

Owing to their low density, large porosity, and high surface area, optical biopolymer aerogels are an exciting class of soft materials for applications in sensing, absorption, insulation, and tissue engineering.[40−42] We found that the prepared water-soluble chitosan is a good polymeric matrix to support the chitosan-functionalized $NaYF_4$:Yb,Er colloids, encouraging us to fabricate $NaYF_4$:Yb,Er/chitosan aerogels. The chitosan-coated $NaYF_4$:Yb,Er colloids and glyoxal cross-linkers were mixed with water-soluble chitosan to form a homogeneous and optically transparent dispersion. These mixtures were thermally gelated at 80 °C to form $NaYF_4$:Yb,Er/chitosan hydrogels (Figure S5). The removal of water in the hydrogels by freeze-drying yielded intact $NaYF_4$:Yb,Er/chitosan aerogel composites (Figure 2b, right). Under lyophilization, the frozen $NaYF_4$:Yb,Er/chitosan hydrogels released water by sublimation to leave large interconnected interspaces in solidified networks, forming $NaYF_4$:Yb,Er/chitosan aerogels. The aerogel structure appears to be a homogeneous porous network of highly interconnected chitosan nanofibrils, where no phase separation of the $NaYF_4$:Yb,Er nanoparticles is observed, indicating a good distribution of the UC guests into the biopolymer host.

The aerogel composite is a heterogeneous mixture of α,β-$NaYF_4$:Yb,Er crystals and chitosan polymorphs (PXRD, Figure 2e). The aerogel composites are thermally stable up to ∼300 °C, above which chitosan is decomposed to leave ∼10 wt % of oxidized $NaYF_4$:Yb,Er component (thermogravimetric analysis (TGA), Figure S6). SEM images (Figure 2d) of the aerogel composites show the random distribution of the $NaYF_4$:Yb,Er nanorods in the aerogel networks of the solidified chitosan assemblies. These results reveal that the glyoxal-crosslinked

DOI: 10.1021/acsomega.7b01355
ACS Omega 2018, 3, 86−95

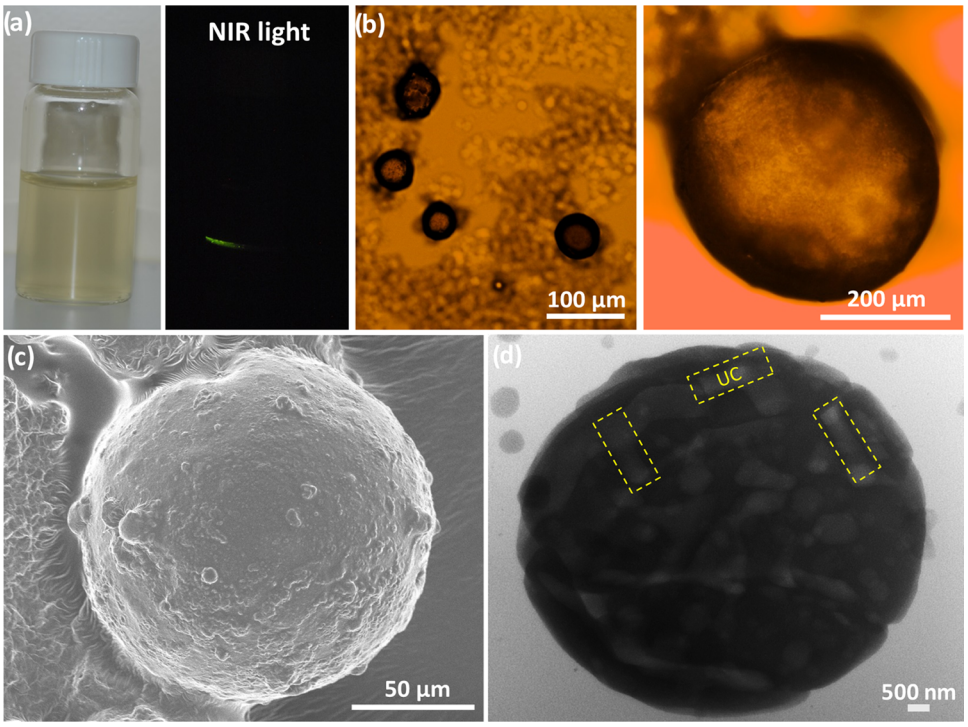

Figure 3. Self-assembly of $NaYF_4$:Yb,Er UC hexagonal nanorods with water-soluble chitosan into microspheres. (a) Photos of UC/chitosan microsphere aqueous dispersion under visible light (left) and NIR light (right), (b) optical microscopy images of UC/chitosan microspheres in the microemulsion dispersion (left) and aqueous media (right), and (c) SEM image and (d) TEM image of UC/chitosan microspheres.

gelation of $NaYF_4$:Yb,Er/chitosan aqueous dispersions occurs upon curing to form gel composites. Nitrogen adsorption−desorption isotherms of the $NaYF_4$:Yb,Er/chitosan composites show a mesoporous structure, indicative of forming macro−mesoporous networks in the aerogels (Figure S6a). Laser excitation of the composites at 980 nm emits visible green light through the aerogels, reflecting a good guest/host combination (Figure 2b, left). Photoluminescence spectra (Figure 2f) of the aerogels show UC emission peaks, with the wavelengths and intensities mostly resembling those of the pristine $NaYF_4$:Yb,Er nanocrystals, suggesting that the sequential gelation and solidification of water-soluble chitosan retain the optical properties of the UC nanoparticles. Although many nanostructures of luminescent chitosan composite gels based on nanocarbons[43−45] and nanosemiconductors,[46,47] for example, have been reported, this is the first preparation of the upconverting $NaYF_4$:Yb,Er/chitosan aerogels. Apart from their promising biomedical applications, the enlarged porous networks may facilitate the diffusion of volatile reactants to make the UC/chitosan aerogels useful as gas optical sensors.[48]

Optical biopolymer microsphere colloids have aroused attention for applications in drug delivery.[49,50] Keeping this demand in mind, we further explored the fabrication of $NaYF_4$:Yb,Er/chitosan microspheres. In general, the $NaYF_4$:Yb,Er/chitosan aqueous dispersions can self-organize into microspheres via microemulsion-assisted assembly, where the optical guests are embedded within the chitosan host. The synthesis involves a precursor aqueous phase confined in an oil/surfactant phase. The precursor aqueous phase was prepared by mixing the chitosan-stabilized $NaYF_4$:Yb,Er aqueous dispersion and glyoxal with water-soluble chitosan to form a homogeneous mixture. The solvent (oil) phase was prepared by dissolving Span 80 surfactant in paraffin. An emulsion system was prepared by mixing these phases together under sequential stirring and sonication. The emulsion mixture was transferred into a round-bottomed flask, sealed, and then heated to 80 °C under moderate stirring to crosslink chitosan by glyoxal, producing solidified $NaYF_4$:Yb,Er/chitosan microspheres. We first examined the synthesized materials using optical microscopy. It is apparent from the optical images that both the solidified products before and after purification are dispersible microspheres (Figure 3b).

The solidified microspheres were collected and dispersed in water to form a microsphere aqueous solution (Figure 3a, left). On shining the 980 nm laser light through the samples, the solidified products and their aqueous solutions both emit green light (Figure 3a, right). Structural and elemental analyses reveal that the solidified product is a heterogeneous mixture of α,β-$NaYF_4$:Yb,Er nanocrystals and chitosan polymorphs (PXRD, Figure S7a). Thermal analyses (Figure S7b) confirm ∼5 wt % $NaYF_4$:Yb,Er in the chitosan-based composites. Photoluminescence spectrum (Figure S8) of the microsphere composites shows the retention of the spectral features of the pristine $NaYF_4$:Yb,Er nanorods. SEM images (Figures 3c and S9) of the solidified products show a broad size distribution of microspheres in the diameter range of 150−200 μm. The $NaYF_4$:Yb,Er nanorods embedded within the chitosan microspheres seem to be distinguished by TEM, as presented in Figures 3d and S10. These analyses confirm the formation of the photoluminescent $NaYF_4$:Yb,Er/chitosan microspheres in the microemulsion system with the assistance of the Span 80 nonionic surfactant. In the oil/water phases, the hydrophobic alkyl tails of the surfactant move forward to the oil phase (paraffin), whereas its hydrophilic oleate heads (functional groups) move forward oppositely to the aqueous phase (water). This chemical behavior leads to the formation of stable sphere-shaped micelles containing $NaYF_4$:Yb,Er/chitosan aqueous hydrogels confined within the paraffin oil phase. Under glyoxal

DOI: 10.1021/acsomega.7b01355
ACS Omega 2018, 3, 86−95

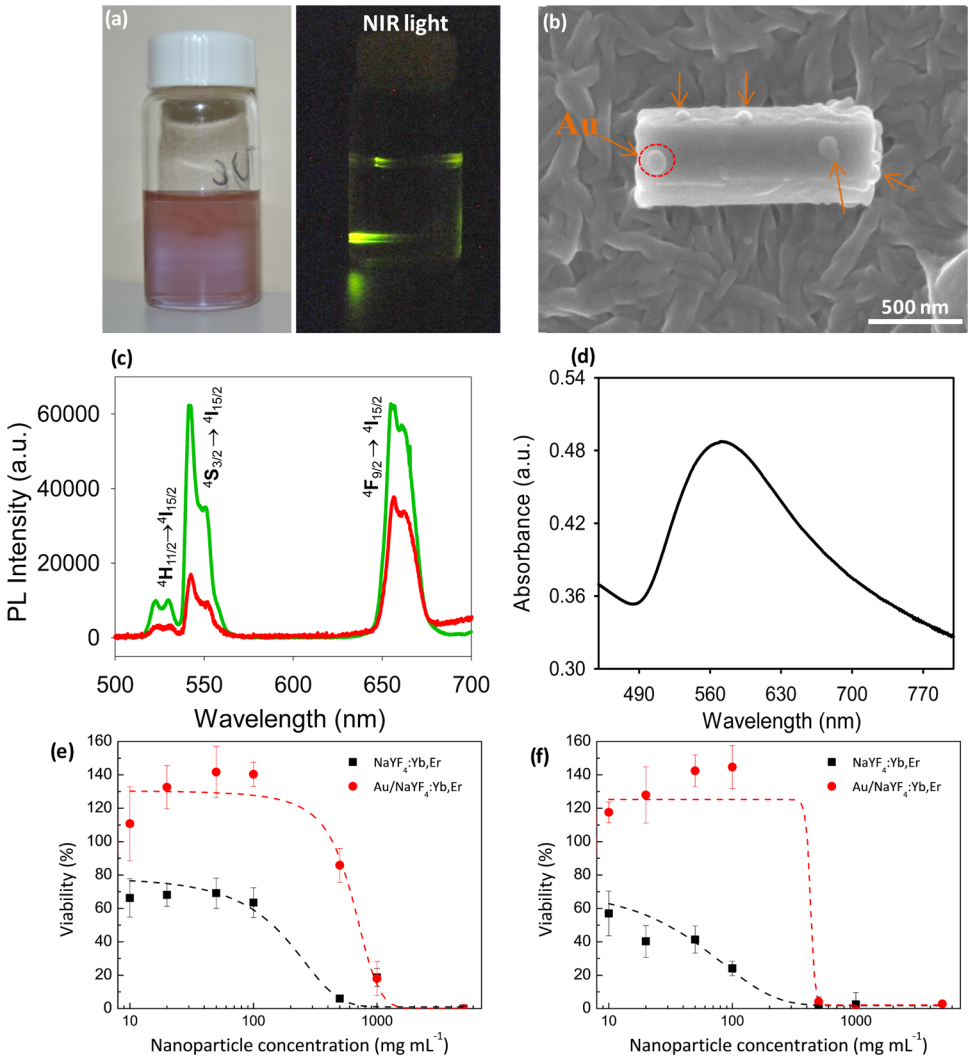

Figure 4. Water-soluble chitosan-stabilized Au/$NaYF_4$:Yb,Er nanocomposites and their dose-dependent cytotoxicity. (a) Photos of chitosan-stabilized Au/$NaYF_4$:Yb,Er nanocomposite aqueous dispersion under visible light (left) and NIR light (right), (b) SEM image of Au/$NaYF_4$:Yb,Er nanocomposites, (c) UC photoluminescence spectra of Au/$NaYF_4$:Yb,Er nanocomposites (green) in comparison to those of $NaYF_4$:Yb,Er hexagonal nanorods (red), (d) UV−vis absorption spectrum of Au/$NaYF_4$:Yb,Er nanocomposites and WST-1 viability assay of chitosan-stabilized Au/$NaYF_4$:Yb,Er nanocomposites in comparison to those of chitosan-stabilized $NaYF_4$:Yb,Er hexagonal nanorods after 24 h (e) and 72 h (f).

crosslinking and curing, the $NaYF_4$:Yb,Er-supported chitosan networks can be crosslinked to form rigid hydrogel microspheres. Although several examples have recently been reported for chitosan spheres, to the best of our knowledge, this is the first combination of $NaYF_4$:Yb,Er UC nanoparticles and water-soluble chitosan into the biocompatible optical microsphere colloids.

The structural design of the nanomaterials with multioptical properties is also a goal to enhance their desirable functionalities.[27,51] We realized that the well-defined anisotropic shape and good dispersity can lead the $NaYF_4$:Yb,Er hexagonal nanorods to serve as an efficient UC support for plasmonic additives. In a typical preparation, a $HAuCl_4$ ethylene glycol solution was mixed with an OA-capped $NaYF_4$:Yb,Er ethanol dispersion under stirring to form a homogeneous mixture. These mixed dispersions were hydrothermally treated at 80 °C to prepare Au/$NaYF_4$:Er,Yb nanocomposites. The reaction mixtures slowly turned from yellow to purple upon heating, indicating the formation of Au nanoparticles (Figure 4a). PXRD analyses reveal the structural retention of α,β-$NaYF_4$ crystals in the nanocomposites, and the Au component could not be detected, possibly due to its low loading concentration (Figure S12). However, electron microscope images (Figure 4b) show the surface deposition of some uniform Au nanodots with ∼50 nm particle size on the single $NaYF_4$:Er,Yb nanorods. These structural analyses confirm the selective decoration of the Au nanoparticles on the $NaYF_4$:Yb,Er hexagonal nanorods to generate plasmonic upconverting nanohybrids.

Ethylene glycol can act as a weak reductant to perform the polyol-assisted reduction of some metal ions under hydrothermal conditions. At elevated temperature, ethylene glycol is able to slowly reduce Au^{3+} into small Au nanoparticles, which are then attached on the $NaYF_4$:Er,Yb nanorods. The weak reduction allows one to control the growth and size distribution of the Au nanodots in the nanocomposites. This hydrothermal polyol reduction provides an advantage over conventional methods, which often use strong reductants such as $NaBH_4$ or ascorbic acid to obtain deposited Au nanoparticles with larger irregular sizes, as additionally evidenced in Figure S14. The UC emission peaks of the Au/$NaYF_4$:Yb,Er nanocomposites have the same wavelengths as those of the pristine $NaYF_4$:Yb,Er

DOI: 10.1021/acsomega.7b01355
ACS Omega 2018, 3, 86−95

nanorods (three maxima at 522.5, 541.5, and 655.5 nm); however, their spectral emission has a significantly higher intensity (Figure 4c). UV−vis spectra (Figure 4d) of the Au/$NaYF_4$:Yb,Er nanocomposites show a maximum plasmon absorbance at ∼540 nm for the Au nanoparticles. The plasmon-enhanced upconverting photoluminescence in the Au/$NaYF_4$:Yb,Er nanocomposites may be caused by the plasmon−photon coupling effect, as recently reported elsewhere.[52,53]

To explore the biomedical compatibility, we further prepared chitosan-stabilized Au/$NaYF_4$:Yb,Er nanocomposites by dispersing the ethylene glycol-capped Au/$NaYF_4$:Yb,Er nanocomposites in water-soluble chitosan. A stable colloidal solution of the Au/$NaYF_4$:Yb,Er nanohybrids can be obtained after sonication (Figure 4a). Again, the aqueous stability of these nanocomposite colloids is due to the surface adsorption of water-soluble chitosan. The chitosan-stabilized Au/$NaYF_4$:Yb,Er nanocomposites maintain the morphological integrity of the pristine samples (Figure S15).

We investigated the cytotoxic response of the chitosan-stabilized Au/$NaYF_4$:Yb,Er nanocomposites (Figure 4a) in comparison to that of the chitosan-stabilized $NaYF_4$:Yb,Er nanoparticles (Figure S11) to assess their suitability for biomedical diagnosis. In this sense, the lack of the functional moieties on the UC nanoparticle surfaces is often an obstacle that needs to be addressed for biomedical applications. To date, the UC nanoparticles have been coated with silica, sodium gluconate, poly(ethylene glycol), poly(ethylene glycol)−poly(acrylic acid), cationic conjugated polyelectrolytes, phosphatidylcholine, and hyaluronate to improve their biocompatibility.[54−58] Our present work has used native chitosan polycation as a water-soluble biopolymer to coat the $NaYF_4$:Yb,Er nanoparticles and Au/$NaYF_4$:Yb,Er nanohybrids for generating the novel biocompatible optical composites.[22]

Figure 4e,f shows the cytotoxic response of these materials. The experimental results were performed by incubating different concentrations of nanoparticles from 10 to 5000 μg mL^{-1} with living cells in culture for 24 and 72 h. The dose response for the chitosan-stabilized $NaYF_4$:Yb,Er nanoparticles presents half-maximal effective concentrations (EC_{50}) of 240 and 96 μg mL^{-1} after 24 and 72 h, respectively. After Au deposition, the respective EC_{50} value is notably increased to 580 and 410 μg mL^{-1}, respectively. The high cell viability of the chitosan-stabilized Au/$NaYF_4$:Yb,Er nanocomposites is remarkable, which is found to be more than 80% when incubated for 24 h at the concentration of 500 μg mL^{-1}. Overall, these UC nanocomposites present enhanced biocompatibility in comparison to that reported in previous works.[59] This enhancement may arise from the chitosan coating to avoid the possible release of toxic lanthanide ions to the surrounding cellular environment.[60] Indeed, Tian et al.[61] proved that ligand-free lanthanide-doped nanoparticles are cytotoxic because of the cellular adenosine triphosphate deprivation of cells. These UC nanoparticles induced cell death through autophagy and apoptosis because of the interactions between the particles and phosphate groups. They concluded that the best practice is to limit the concentration of the UC nanoparticles below 100 μg mL^{-1}, which is high enough to ensure proper cell imaging and still far below the EC_{50} here obtained after 24 h.

The NIR response, aqueous dispersity, biocompatibility, and low cytotoxicity reported here indicate that the chitosan-stabilized Au/$NaYF_4$:Yb,Er nanohybrids may be useful as a promising bioprobe for the imaging of tissues with minimal cell damage.[62] Additionally, recent studies have shown that the plasmonic upconverting coupling at the nanoscale may induce photothermal effects by direct laser irradiation through luminescence resonance emission transfer from $NaYF_4$:Yb,Er to Au.[63] This photon transfer behavior also makes these hybrid nanoparticles interesting for exploiting hyperthermia therapy.

3. CONCLUSIONS

In summary, we have shown the fabrication of biocompatible chitosan-functionalized optical nanocomposites based on near-infrared-sensitive upconverting nanoparticles. Hydrophobic $NaYF_4$:Yb,Er hexagonal nanorods synthesized by hydrothermolysis were used as a photon upconverter. Water-soluble chitosan was prepared by acetylation of native chitosan nanofibrils and used to functionalize the $NaYF_4$:Yb,Er nanocrystals into biocompatible optical nanomaterials. The novelty of the aqueous solubility and polymorphs led water-soluble chitosan to serve as a stabilizer, gel matrix, and spherical support for the upconverting nanomaterials. This homogeneous combination allowed us to design the upconverting nanocomposites with different structures of aqueous colloid, aerogel, microsphere, and hybrid. The simultaneous integration of NIR response and biocompatibility endows the optical materials with biofunctionality, as we have demonstrated the low cytotoxic response of the chitosan-stabilized Au/$NaYF_4$:Yb,Er nanocomposites. These novel materials are useful for extended studies in biomedicine, bioimaging, drug delivery, and analytical sensing.

4. EXPERIMENTAL SECTION

4.1. Preparation of $NaYF_4$:Yb,Er Upconverting Nanocrystals. An aqueous basic mixture of ionic coprecursors (lanthanide and fluoride with the desired concentration) and 0.23 g of NaOH, 4.73 g of oleic acid, 6.6 mL of ethanol, and 1.0 mL of water was prepared under vigorous stirring until a translucent solution was obtained. The reaction mixture was transferred into a Teflon-lined autoclave and heated to 190 °C. After the hydrothermal treatment for 24 h, the white product that precipitated out of the mixture was collected at the bottom of the autoclave. The product was washed with ethanol and harvested by centrifugation to obtain OA-capped $NaYF_4$:Yb,Er upconverting nanocrystals. Hexagonal rod-shaped nanocrystals were formed using lanthanide nitrates (150 mg of $Y(NO_3)_3$, 108 mg of $Yb(NO_3)_3$, and 11 mg of $Er(NO_3)_3$) and 116 mg of NaF, whereas the 2-fold increased precursor concentration formed cube-/rod-shaped nanocrystals.

4.2. Preparation of Water-Soluble Chitosan. Chitin was chemically purified from crab shells by deproteinization and decalcification. The purified chitin (∼25 g) was treated at least twice with a concentrated NaOH aqueous solution (50 wt %, 500 mL) at 90 °C for 8 h to obtain chitosan flakes. The prepared chitosan was immersed in ethanol to remove adsorbed water. The dried chitosan (∼5 g) was added to 40 mL pure acetic anhydride to perform acetylation at room temperature within 4 h. The acetylated chitosan was collected from the reaction solution by filtration, dabbed with tissue paper, and washed quickly with distilled water to remove adsorbed acetic anhydride. The resulting samples were immersed in water to make them swell and then dissolved into a homogeneous chitosan aqueous solution.

4.3. Preparation of $NaYF_4$:Yb,Er/Chitosan Aerogel Composites. OA-capped $NaYF_4$:Yb,Er hexagonal nanorods

DOI: 10.1021/acsomega.7b01355
ACS Omega 2018, 3, 86−95

(~60 mg) were dispersed in 20 mL of water-soluble chitosan (~3 wt %) in the presence of 0.5 mL of glyoxal to form a homogenous mixture after stirring for 1 h. The reaction mixture was hydrothermally treated at 80 °C for 6 h to crosslink chitosan by glyoxal. Upon thermal crosslinking, gelation of the reaction mixture occurred, forming hydrogel composites. The resulting hydrogels were freeze-dried to recover $NaYF_4$:Yb,Er/chitosan aerogel composites.

4.4. Preparation of $NaYF_4$:Yb,Er/Chitosan Microsphere Composites. An aqueous-in-oil microemulsion system was designed to prepare $NaYF_4$:Yb,Er/chitosan microsphere composites. The aqueous phase is ~2 mg of $NaYF_4$:Yb,Er nanorods/1.25 mL of water-soluble chitosan (~3 wt %)/0.1 mL of glyoxal, whereas the oil phase is 1.25 g of Span 80/30 mL paraffin. These phases were mixed together in a flask reactor, forming a cloudy emulsion system after stirring and sonication. The flask reactor was sealed and heated at 80 °C to crosslink chitosan by glyoxal within 48 h. The solidified microspheres were collected by adding 40 mL hexane into the microemulsion, followed by centrifugation. The white solidified product of $NaYF_4$:Yb,Er/chitosan microsphere composites was washed with ethanol and dispersed in water.

4.5. Preparation of Chitosan-Stabilized Au/$NaYF_4$:Yb,Er Nanocomposites. OA-stabilized $NaYF_4$:Yb,Er hexagonal nanorods (~5 mg) were added to 20 mL of ethylene glycol containing 0.01 mg of $HAuCl_4$. The reaction mixture was stirred for 1 h and then hydrothermally treated at 80 °C under stirring for 20 h to form a purple solution. These nanocomposites were collected and purified with Au/$NaYF_4$:Yb,Er nanocomposites with ethanol and then added to water-soluble chitosan (20 mL, ~1 wt %) under stirring and sonication to form a chitosan-stabilized Au/$NaYF_4$:Yb,Er aqueous dispersion.

4.6. Cytotoxicity Assay. Dose-dependent cytotoxicity of chitosan-stabilized $NaYF_4$:Yb,Er nanoparticles and chitosan-stabilized Au/$NaYF_4$:Yb,Er nanocomposites after 24 and 72 h was evaluated according to the WST-1 viability assay. First, the nanoparticles were sterilized by irradiation for 10 min. Then, they were washed by spinning them down at 1000 rpm for 5 min, and the resulting solution was replaced with fresh growth media (MEM-α with glutamax, 1% P/S, 10% fetal bovine serum). DU145 human prostate cancer cells were then seeded in a 96-well plate at a concentration of 1000 cells/well. After 24 h, media in wells were replaced with the nanoparticle media solution at various concentrations ranging from 0.01 to 1 mg mL^{-1}. Positive control wells (100% viability) were established by adding fresh media to a row of cells, whereas negative control wells (0% viability) were established by adding an excessive amount of nanoparticle solution (5 mg mL^{-1}). The EC_{50} of the cells was determined by plotting relative cell viability (relative to positive and negative controls in %) in OriginPro. Each experiment was repeated six times.

■ ASSOCIATED CONTENT

Supporting Information

The Supporting Information is available free of charge on the ACS Publications website at DOI: 10.1021/acsomega.7b01355.

Chemicals, structural characterization, IR, EDX, TGA, PXRD, SEM, TEM, PL spectra, nitrogen adsorption−desorption isotherms, and photos (PDF)

■ AUTHOR INFORMATION

Corresponding Authors

*E-mail: trthaihoa@yahoo.com (H.T.T.).
*E-mail: nguyenvietlong@sgu.edu.vn (L.V.N.).
*E-mail: ntdinhc@chem.ubc.ca (T.-D.N.).

ORCID

Manuel Salmerón-Sánchez: 0000-0002-8112-2100

Present Address

◆L.V.N.: Department of Electronics and Telecommunications, Saigon University, 273 An Duong Vuong Street, Ho Chi Minh 700000, Vietnam

Notes

The authors declare no competing financial interest.

■ ACKNOWLEDGMENTS

We are grateful to the National Foundation for Science and Technology Development of Vietnam under grant number 104.06-2014.87 for funding. H.V.D. thanks financial support from the Hue University Foundation Programme (DHH 2016-02-83). M.S.S. acknowledges support from EPSRC (EP/P001114/1).

■ REFERENCES

(1) Zhou, J.; Yang, Y.; Zhang, C. Y. Toward biocompatible semiconductor quantum dots: from biosynthesis and bioconjugation to biomedical application. *Chem. Rev.* **2015**, *115*, 11669−11717.

(2) Yao, J.; Yang, M.; Duan, Y. Chemistry, biology, and medicine of fluorescent nanomaterials and related systems: new insights into biosensing, bioimaging, genomics, diagnostics, and therapy. *Chem. Rev.* **2014**, *114*, 6130−6178.

(3) Algar, W. R.; Prsuhn, D. E.; Stewart, M. H.; Jennings, T. L.; Canosa, J. B. B.; Dawson, P. E.; Medintz, I. L. The controlled display of biomolecules on nanoparticles: a challenge suited to bioorthogonal chemistry. *Bioconjugate Chem.* **2011**, *22*, 825−858.

(4) Xiang, D.; Wang, X.; Jia, C.; Lee, T.; Guo, X. Molecular-scale electronics: from concept to function. *Chem. Rev.* **2016**, *116*, 4318−4440.

(5) Soenen, S. J.; Parak, W. J.; Rejman, J.; Manshian, B. (Intra)cellular stability of inorganic nanoparticles: effects on cytotoxicity, particle functionality, and biomedical applications. *Chem. Rev.* **2015**, *115*, 2109−2135.

(6) Pihan, S. A.; Emmerling, S. G. J.; Butt, H. J.; Berger, R.; Gutmann, J. S. Soft nanocomposites - from interface control to interphase formation. *ACS Appl. Mater. Interfaces* **2015**, *7*, 12380−12386.

(7) Qin, X.; Liu, X.; Huang, W.; Bettinelli, M.; Liu, X. Lanthanide-activated phosphors based on 4f−5d optical transitions: theoretical and experimental aspects. *Chem. Rev.* **2017**, *117*, 4488−4527.

(8) Stepuk, A.; Casola, G.; Schumacher, C. M.; Kramer, K. W.; Stark, W. J. Purification of $NaYF_4$-based upconversion phosphors. *Chem. Mater.* **2014**, *26*, 2015−2020.

(9) Boles, M. A.; Engel, M.; Talapin, D. V. Self-assembly of colloidal nanocrystals: from intricate structures to functional materials. *Chem. Rev.* **2016**, *116*, 11220−11289.

(10) Zhou, B.; Shi, B.; Jin, D.; Liu, X. Controlling upconversion nanocrystals for emerging applications. *Nat. Nanotechnol.* **2015**, *10*, 924−936.

(11) Wu, X.; Chen, G.; Shen, J.; Li, Z.; Zhang, Y.; Han, G. Upconversion nanoparticles: a versatile solution to multiscale biological imaging. *Bioconjugate Chem.* **2015**, *26*, 166−175.

(12) Zhou, J.; Liu, Q.; Feng, W.; Sun, Y.; Li, F. Upconversion luminescent materials: advances and applications. *Chem. Rev.* **2015**, *115*, 395−465.

(13) Cates, E. L.; Chinnapongse, S. L.; Kim, J. H.; Kim, J. H. Engineering light: advances in wavelength conversion materials for

DOI: 10.1021/acsomega.7b01355
ACS Omega 2018, 3, 86−95

energy and environmental technologies. *Environ. Sci. Technol.* **2012**, *46*, 12316−12328.
(14) Dong, H.; Du, S. R.; Zheng, X. Y.; Lyu, G. M.; Sun, L. D.; Li, L. D.; Zhang, P. Z.; Zhang, C.; Yan, C. H. Lanthanide nanoparticles: from design toward bioimaging and therapy. *Chem. Rev.* **2015**, *115*, 10725−10815.
(15) Andrés, E.; Jove, D. A.; Biarnes, X.; Moerschbacher, B. M.; Guernin, M. E.; Planas, A. Structural basis of chitin oligosaccharide deacetylation. *Angew. Chem., Int. Ed.* **2014**, *53*, 6882−6887.
(16) Liu, R.; Xu, C.; Zhang, Q.; Wang, S.; Fang, W. Evolution of the chitin synthase gene family correlates with fungal morphogenesis and adaption to ecological niches. *Sci. Rep.* **2017**, *7*, No. 44527.
(17) Konwar, A.; Kalita, S.; Kotoky, J.; Chowdhury, D. Chitosan-iron oxide coated graphene oxide nanocomposite hydrogel: a robust and soft antimicrobial biofilm. *ACS Appl. Mater. Interfaces* **2016**, *8*, 20625−20634.
(18) Fernandez, J. G.; Ingber, D. E. Manufacturing of large-scale functional objects using biodegradable chitosan bioplastic. *Macromol. Mater. Eng.* **2014**, *299*, 932−938.
(19) Araki, J.; Yamanaka, Y.; Ohkawa, K. Chitin-chitosan nanocomposite gels: reinforcement of chitosan hydrogels with rod-like chitin nanowhiskers. *Polym. J.* **2012**, *44*, 713−717.
(20) Karimi, A. R.; Khodadadi, A. Mechanically robust 3d nanostructure chitosan-based hydrogels with autonomic self-healing properties. *ACS Appl. Mater. Interfaces* **2016**, *8*, 27254−27263.
(21) Colombo, E.; Li, W.; Bhangu, S. K.; Ashokkumar, M. Chitosan microspheres as a template for TiO_2 and ZnO microparticles: studies on mechanism, functionalization and applications in photocatalysis and H_2S removal. *RSC Adv.* **2017**, *7*, 19373−19383.
(22) Chen, Q.; Wang, X.; Chen, F.; Zhang, Q.; Dong, B.; Yang, H.; Liu, G.; Zhu, Y. Functionalization of upconverted luminescent $NaYF_4$:Yb/Er nanocrystals by folic acid-chitosan conjugates for targeted lung cancer cell imaging. *J. Mater. Chem.* **2011**, *21*, 7661−7667.
(23) Kubota, N.; Eguchi, Y. Facile preparation of water-solution N-acetylated chitosan and molecular weight dependence of its water-solubility. *Polym. J.* **1997**, *29*, 123−127.
(24) Wang, J.; Qiu, F.; Wu, H.; Li, X.; Zhang, T.; Niu, X.; Yang, D.; Pan, J.; Xu, J. Novel water-soluble chitosan linked fluorescent carbon dots and isophorone diisocyanate fluorescent material toward detection of chromium(VI). *Anal. Methods* **2016**, *8*, 8554−8565.
(25) Zhang, J.; Xia, W.; Liu, P.; Cheng, Q.; Tahi, T.; Gu, W.; Li, B. Chitosan modification and pharmaceutical/biomedical applications. *Mar. Drugs* **2010**, *8*, 1962−1987.
(26) Duan, J.; Liang, X.; Cao, Y.; Wang, S.; Zhang, L. High strength chitosan hydrogels with biocompatibility via new avenue based on constructing nanofibrous architecture. *Macromolecules* **2015**, *48*, 2706−2714.
(27) Wu, D. M.; Etxarri, A. G.; Salleo, A.; Dionne, J. A. Plasmon-enhanced upconversion. *J. Phys. Chem. Lett.* **2014**, *5*, 4020−4031.
(28) Cui, S.; Chen, H.; Zhu, H.; Tian, J.; Chi, X.; Qian, Z.; Achilefu, S.; Gu, Y. Amphiphilic chitosan modified upconversion nanoparticles for in vivo photodynamic therapy induced by near-infrared light. *J. Mater. Chem.* **2012**, *22*, 4861−4873.
(29) Zhou, A.; Wei, Y.; Wu, B.; Chen, Q.; Xing, D. Pyropheophorbide A and c(RGDyK) comodified chitosan-wrapped upconversion nanoparticle for targeted near-infrared photodynamic therapy. *Mol. Pharmaceutics* **2012**, *9*, 1580−1589.
(30) Chen, C.; Li, C.; Shi, Z. Current advances in lanthanide-doped upconversion nanostructures for detection and bioapplication. *Adv. Sci.* **2016**, *3*, No. 1600029.
(31) Kirch, J.; Schneider, A.; Abou, B.; Hopf, A.; Schaefer, U. F.; Schneider, M.; Schall, C.; Wagner, C.; Lehr, C. M. Optical tweezers reveal relationship between microstructure and nanoparticle penetration of pulmonary mucus. *Proc. Natl. Acad. Sci. U.S.A.* **2012**, *109*, 18355−18360.
(32) Shin, K.; Jung, T.; Lee, E.; Lee, G.; Goh, Y.; Heo, J.; Jung, M.; Jo, E. J.; Lee, H.; Kim, M. G.; Lee, K. T. Distinct mechanisms for the upconversion of $NaYF_4$:Yb^{3+},Er^{3+} nanoparticles revealed by stimulated emission depletion. *Phys. Chem. Chem. Phys.* **2017**, *19*, 9739−9744.
(33) Wilhelm, S. Perspectives for upconverting nanoparticles. *ACS Nano* **2017**, 10644−10653.
(34) Li, M.; Zhen, Z.; Zheng, Y.; Cui, C.; Li, C.; Li, Z. Controlled growth of metal-organic framework on upconversion nanocrystals for NIR-enhanced photocatalysis. *ACS Appl. Mater. Interfaces* **2017**, *9*, 2899−2905.
(35) Wang, M.; Zhu, Y.; Mao, C. Synthesis of NIR-responsive $NaYF_4$:Yb,Er upconversion fluorescent nanoparticles using an optimized solvothermal method and their applications in enhanced development of latent fingerprints on various smooth substrates. *Langmuir* **2015**, *31*, 7084−7090.
(36) Scheucher, E.; Wilhelm, S.; Wolhelm, S.; Hirsch, T.; Mayr, T. Composite particles with magnetic properties, near-infrared excitation, and far-red emission for luminescence-based oxygen sensing. *Microsyst. Nanoeng.* **2015**, *1*, No. 15026.
(37) Song, C.; Zhang, S.; Zhou, Q.; Shi, L.; Du, L.; Zhi, D.; Zhao, Y.; Zhen, Y.; Zhao, D. Bifunctional cationic solid lipid nanoparticles of *β*-$NaYF_4$:Yb,Er upconversion nanoparticles coated with a lipid for bioimaging and gene delivery. *RSC Adv.* **2017**, *7*, 26633−26639.
(38) Yan, C.; Dadvand, A.; Rosei, F.; Perepichka, D. F. Near-IR photoresponse in new up-converting CdSe/$NaYF_4$:Yb,Er nanoheterostructures. *J. Am. Chem. Soc.* **2010**, *132*, 8868−8869.
(39) Welsh, E. R.; Schauer, C. L.; Qadri, S. B.; Price, R. P. Chitosan cross-linking with a water-soluble, blocked diisocyanate. 1. Solid state. *Biomacromolecules* **2002**, *3*, 1370−1374.
(40) Worsley, M. A.; Pauzauskie, P. J.; Olson, T. Y.; Biener, J.; Satcher, J. H., Jr.; Baumann, T. F. Synthesis of graphene aerogel with high electrical conductivity. *J. Am. Chem. Soc.* **2010**, *132*, 14067−14069.
(41) Korhonen, J. T.; Kettunen, M.; Ras, R. H. A.; Ikkala, O. Hydrophobic nanocellulose aerogels as floating, sustainable, reusable, and recyclable oil absorbents. *ACS Appl. Mater. Interfaces* **2011**, *3*, 1813−1816.
(42) Chen, W.; Li, S.; Chen, C.; Yan, L. Self-assembly and embedding of nanoparticles by in situ reduced graphene for preparation of a 3D graphene/nanoparticle aerogel. *Adv. Mater.* **2011**, *23*, 5679−5683.
(43) Omidi, M.; Yadegari, A.; Tayebi, L. Wound dressing application of pH-sensitive carbon dots/chitosan hydrogel. *RSC Adv.* **2017**, *7*, 10638−10649.
(44) Wang, H.; Mukherjee, S.; Yi, J.; Banerjee, P.; Chen, Q.; Zhou, S. Biocompatible chitosan-carbon dot hybrid nanogels for NIR-imaging-guided synergistic photothermal-chemo therapy. *ACS Appl. Mater. Interfaces* **2017**, *9*, 18639−18649.
(45) Gogoi, N.; Barooah, M.; Majumdar, G.; Chowdhury, D. Carbon dots rooted agarose hydrogel hybrid platform for optical detection and separation of heavy metal ions. *ACS Appl. Mater. Interfaces* **2015**, *7*, 3058−3067.
(46) Lin, Y.; Zhang, L.; Yao, W.; Qian, H.; Ding, D.; Wu, W.; Jiang, X. Water-soluble chitosan-quantum dot hybrid nanospheres toward bioimaging and biolabeling. *ACS Appl. Mater. Interfaces* **2011**, *3*, 995−1002.
(47) Mansur, A. A. P.; Mansur, H. S.; Araujo, A. S.; Lobato, Z. I. P. Fluorescent nanohybrids based on quantum dot-chitosan-antibody as potential cancer biomarkers. *ACS Appl. Mater. Interfaces* **2014**, *6*, 11403−11412.
(48) Green, K. K.; Wirth, J.; Lim, S. F. Nanoplasmonic upconverting nanoparticles as orientation sensors for single particle microscopy. *Sci. Rep.* **2017**, *7*, No. 762.
(49) Fan, R.; Li, X.; Deng, J.; Gao, X.; Zhou, L.; Zheng, Y.; Tong, A.; Zhang, X.; You, C.; Guo, G. Dual drug loaded biodegradable nanofibrous microsphere for improving anti-colon cancer activity. *Sci. Rep.* **2016**, *6*, No. 28373.
(50) Li, W.; Zaloga, J.; Ding, Y.; Liu, Y.; Janko, C.; Pischetsrieder, M.; Alexiou, C.; Boccaccini, A. R. Facile preparation of multifunctional superparamagnetic PHBV microspheres containing spions for biomedical applications. *Sci. Rep.* **2016**, *6*, No. 23140.

DOI: 10.1021/acsomega.7b01355
ACS Omega 2018, 3, 86−95

(51) Chen, G.; Qiu, H.; Prasad, P. N.; Chen, X. Upconversion nanoparticles: design, nanochemistry, and applications in theranostics. *Chem. Rev.* **2014**, *114*, 5161−5214.
(52) Wang, Y. L.; Estakhri, N. M.; Johnson, A.; Li, H. Y.; Xu, L. X.; Zhang, Z.; Alu, A.; Wang, Q. Q.; Shih, C. K. Tailoring plasmonic enhanced upconversion in single $NaYF_4:Yb^{3+}/Er^{3+}$ nanocrystals. *Sci. Rep.* **2015**, *5*, No. 10196.
(53) Park, K.; Jung, K.; Kwon, S. J.; Jang, H. S.; Byun, D.; Han, I. K.; Ko, H. Plasmonic nanowire-enhanced upconversion luminescence for anticounterfeit devices. *Adv. Funct. Mater.* **2016**, *26*, 7836−7846.
(54) Ma, D.; Meng, L.; Chen, Y.; Hu, M.; Chen, Y.; Huang, C.; Shang, J.; Wang, R.; Gou, Y.; Yang, J. $NaGdF_4:Yb^{3+}/Er^{3+}$@ $NaGdF_4:Nd^{3+}$@sodium-gluconate: multifunctional and biocompatible ultrasmall core-shell nanohybrids for UCL/MR/CT multimodal imaging. *ACS Appl. Mater. Interfaces* **2015**, *7*, 16257−16265.
(55) Wen, H. Q.; Peng, H. Y.; Liu, K.; Bian, M. H.; Xu, Y. J.; Dong, L.; Yan, X.; Xu, W. P.; Tao, W.; Shen, J. L.; Lu, Y.; Qian, H. S. Sequential growth of $NaYF_4:Yb/Er@NaGdF_4$ nanodumbbells for dual-modality fluorescence and magnetic resonance imaging. *ACS Appl. Mater. Interfaces* **2017**, *9*, 9226−9232.
(56) Hu, W.; Lu, X.; Jiang, R.; Fan, Q.; Zhao, H.; Deng, W.; Zhang, L.; Huang, L.; Huang, W. Water-soluble conjugated polyelectrolyte brush encapsulated rare-earth ion doped nanoparticles with dual-upconversion properties for multicolor cell imaging. *Chem. Commun.* **2013**, *49*, 9012−9014.
(57) Zou, X.; Xu, M.; Yuan, W.; Wang, Q.; Shi, Y.; Feng, W.; Li, F. A water-dispersible dye-sensitized upconversion nanocomposite modified with phosphatidylcholine for lymphatic imaging. *Chem. Commun.* **2016**, *52*, 13389−13392.
(58) Zhang, R.; Lv, K.; Wang, B.; Li, L.; Wang, B.; Liu, M.; Guo, H.; Wang, A.; Lu, Y. Design, synthesis and antitubercular evaluation of benzothiazinones containing an oximido or amino nitrogen heterocycle moiety. *RSC Adv.* **2017**, *7*, 1480−1483.
(59) Becerro, A. I.; Mancebo, D. G.; Cantelar, E.; Cusso, F.; Stepien, G.; Fuente, J. M.; Ocana, M. Ligand-free synthesis of tunable size $Ln:BaGdF_5$ (Ln = Eu^{3+} and Nd^{3+}) nanoparticles: luminescence, magnetic properties, and biocompatibility. *Langmuir* **2016**, *32*, 411−420.
(60) Liu, Y.; Zhan, S.; Yang, Q.; Yan, M. Synthesis of biocompatible uniform $NaYF_4:Yb^{3+},Er^{3+}$ nanocrystals and their characteristic photoluminescence. *J. Lumin.* **2012**, *132*, 3042−3047.
(61) Tian, J.; Zeng, X.; Xie, X.; Han, S.; Liew, Q. W.; Chen, Y. T.; Wang, L.; Liu, X. Intracellular adenosine triphosphate deprivation through lanthanide-doped nanoparticles. *J. Am. Chem. Soc.* **2015**, *137*, 6550−6558.
(62) König, K. Laser tweezers and multiphoton microscopes in life sciences. *Histochem. Cell Biol.* **2000**, *114*, 79−92.
(63) Chen, C. W.; Lee, P. H.; Chan, Y. C.; Hsiao, M.; Chen, C. H.; Wu, P. C.; Wu, P. R.; Tsai, D. P.; Tu, D.; Chen, X.; Liu, R. S. Plasmon-induced hyperthermia: hybrid upconversion $NaYF_4:Yb/Er$ and gold nanomaterials for oral cancer photothermal therapy. *J. Mater. Chem. B* **2015**, *3*, 8293−8302.

DOI: 10.1021/acsomega.7b01355
ACS Omega 2018, 3, 86−95